

Electrical properties of yttrium iron garnet at high temperatures

P. K. Larsen and R. Metselaar

Philips Research Laboratories, Eindhoven, The Netherlands

(Received 26 February 1976)

The dc electrical conductivity (σ) and the Seebeck coefficient (α) have been measured on *n*- and *p*-type single crystals of yttrium iron garnet (YIG) in the temperature range 600–1500 K. The temperature dependence of σ and α at an oxygen partial pressure (P_{O_2}) of 1 atm shows extrinsic behavior of σ for both *n*- and *p*-type samples with a thermal generation of charge carriers as the main cause of the temperature dependence of σ . The intrinsic conductivity was studied at various temperatures by measurements on *p*-type samples under a low P_{O_2} . A compilation of the experimental data in an α - σ plot shows consistency between the measurements on different samples. An analysis of the experimental results leads to the temperature-independent relations $\mu_+ N_+ e^{A_+} = 3.0 \times 10^{21} (\text{V sec cm})^{-1}$ and $\mu_- N_- e^{A_-} = 5.2 \times 10^{20} (\text{V sec cm})^{-1}$ for holes (+) and electrons (-), where μ , N , and A are the drift mobility, the effective density of states, and the transport coefficient, respectively. Further results are the relations $\beta/k + A_+ + A_- = -5.4$, and $A_- + \ln(g_-) = 2.7$, where the constant β determines the temperature dependence of the band-gap energy, and g_- is the spin degeneracy factor of Si impurities in YIG. The results are discussed in terms of the localized hopping model for YIG, the small-polaron model, and the large-polaron model. For both *n*- and *p*-type YIG the large-polaron model is in best agreement with the results.

I. INTRODUCTION

This paper describes an investigation of the electrical transport properties of yttrium iron garnet, $\text{Y}_3\text{Fe}_5\text{O}_{12}$ (YIG). Many investigations have been concerned with the magnetic, optical, and magneto-optical properties of YIG, which serves as a model compound for this class of materials. So far, however, very few investigations have provided real insight into the electrical transport properties of this compound. From measurements of the Seebeck coefficient Verweel and Rovers showed that polycrystalline YIG samples could be made *n*-type by Si-doping and *p*-type by Ca doping.¹ The influence of divalent and tetravalent substitutions on the optical-absorption coefficient was shown by Wood and Remeika.² The results of these optical-absorption measurements and of numerous low-temperature experiments on photomagnetic effects^{3,4} were explained by assuming that Fe^{2+} ions are formed when tetravalent ions are substituted for part of the trivalent ions. Correspondingly, substituted divalent ions were assumed to be compensated by Fe^{4+} ions.

In this localized picture the electrical conductivity of YIG is ascribed to a hopping type of conduction. For *n*-type materials the number of Fe^{2+} ions equals the effective donor concentration, while the temperature dependence of the conductivity is ascribed to the temperature dependence of the mobility of the ferrous ions. The measurements of the Seebeck coefficient and the conductivity of Hf-doped YIG by Elwell and Dixon are consistent with this picture.⁵ A similar conclusion was reached by Ksendzov *et al.* for a Si-doped YIG

crystal.⁶ Contrary to these results measurements of the Hall mobility in Si-doped YIG by Fontana and Epstein did not show any temperature dependence, and therefore these authors concluded that *n*-type YIG shows band conduction.⁷ The present authors demonstrated by a study of inhomogeneous conduction in polycrystalline *n*-type YIG in the space-charge-limited conduction region, that differences in conduction between grains and grain boundaries could mainly be attributed to a difference in the position of the Fermi level (measured relative to the bands) and only to a small extent to a difference in the mobility.⁸ These disparate results emphasize the need for further investigation of the transport properties of *n*-type YIG. So far, no systematic studies of the transport properties of *p*-type YIG have been performed. However, a recent photoemission study gives a strong indication for the absence of localized bands as the uppermost filled bands and therefore proposes band conduction in *p*-type YIG.⁹

In this paper we make use of the method of combined plots of Seebeck voltages and conductivity. As suggested by Jonker¹⁰ this method is particularly useful for comparing the results obtained on different samples. Our measurements were performed in the temperature range 600–1500 K (Curie temperature $T_C = 562$ K) on single crystals with different dopants. We have shown earlier that the electrical conductivity at high temperatures is not determined by the concentrations of foreign acceptors and donors only, but is strongly influenced by the concentration of oxygen vacancies which act as donors.¹¹ By varying the oxygen partial pressure at high temperatures we can easily change

the concentration of oxygen vacancies. We have made use of this to determine the band-gap energy E_g ($T=0$ K) of YIG.¹¹ From the response of the conductivity to a change in the oxygen partial pressure we have also measured the oxygen diffusion coefficient.¹²

In Sec. II of this paper we present the method used to analyze the transport properties, with the appropriate equations. The experimental method will be outlined in Sec. III, followed by a presentation of the experimental results (Sec. IV). A subsequent analysis of measurements is given in Sec. V. Finally, our results will be discussed in terms of different models in the concluding Sec. VI.

II. METHOD OF ANALYSIS

In this section we give some general equations for the dc conductivity and thermoelectric power.

We assume a semiconductor with a band-gap energy E_g , effective densities of states N_+ and N_- , drift mobilities μ_+ and μ_- , and transport coefficients A_+ and A_- . Here the subscripts “+” and “-” refer to the valence band and conduction band, respectively. Let the concentrations of charge carriers in the valence and conduction band be p and n . The conductivity σ is the sum of the contributions from two bands, σ_+ and σ_- , respectively,

$$\sigma = \sigma_+ + \sigma_- = p e \mu_+ + n e \mu_-, \quad (1)$$

where n and p are related by

$$np = N_+ N_- e^{-E_g/kT}. \quad (2)$$

The Seebeck coefficient α can be expressed in the partial Seebeck coefficients α_+ and α_- via

$$\alpha = (\sigma_+ \alpha_+ + \sigma_- \alpha_-) / (\sigma_+ + \sigma_-), \quad (3)$$

where

$$\alpha_+ = (k/e)[A_+ + \ln(N_+/p)] \quad (4a)$$

and

$$\alpha_- = -(k/e)[A_- + \ln(N_-/n)]. \quad (4b)$$

In these expressions e is the absolute value of the electronic charge.

In the so-called extrinsic conduction range σ and α are dominated by the contribution of only one type of charge carrier, e.g., when the holes are the majority carriers $\sigma \approx \sigma_+$ and $\alpha \approx \alpha_+$. In that case, we have from Eq. (4a)

$$\alpha' = \alpha e / k \ln 10 = A_+ / \ln 10 + \log_{10}(N_+/p). \quad (5a)$$

For the resistivity ρ in the extrinsic p -type conduction region we have from Eq. (1)

$$\log_{10} \rho = -\log_{10}(p e \mu_+). \quad (5b)$$

If the product $N_+ \mu_+$ is temperature independent,

which is generally the case for band conduction, Eqs. (5a) and (5b) show that plots of $\log_{10} \rho$ and of α' vs T^{-1} give straight lines with equal slopes. When the mobility is thermally activated, there will be a difference in the slopes of the two lines.

Since $p = N_+ \exp[(E_V - E_F)/kT]$, where E_V and E_F denote the energies of the top of the valence band and the Fermi level, respectively, we can also write

$$\alpha e / k = A_+ + (E_F - E_V) / kT. \quad (6)$$

For a nondegenerate partially compensated p -type semiconductor the temperature dependence of E_F for $p \ll N_a - N_d$ can be approximated with¹³

$$E_F - E_V = E_a - kT \ln[(N_a - N_d) / g_+ N_d]. \quad (7)$$

Here E_a is the ionization energy of the acceptors, N_a is the acceptor concentration, N_d the donor concentration, and g_+ is the degeneracy factor of the acceptor center. Combination of Eqs. (6) and (7) shows that

$$\alpha e / k = E_a / kT + \ln(g_+ e^{A_+}) - \ln[(N_a - N_d) / N_d]. \quad (8)$$

So from the slope of the α vs T^{-1} plot we obtain E_a (or E_d for n -type materials). When the degree of compensation is known the intercept of the curve at $T^{-1} = 0$ can be used to determine the product $g e^A$.

When $n \mu_-$ and $p \mu_+$ are of comparable magnitude the conductivity is described by Eq. (1). From Eqs. (1) and (2) it follows that σ reaches a minimum value:

$$\sigma_{\min} = 2e(\mu_+ \mu_- N_+ N_-)^{1/2} e^{-E_g/2kT} e^{-\beta/2k}, \quad (9)$$

where we have assumed a simple linear temperature dependence of E_g , $E_g = E_{g0} + \beta T$. We see that for this case $\sigma_+ = \sigma_- = \frac{1}{2} \sigma_{\min}$. Because the parameters N , μ , and A usually differ for the two types of charge carriers the Seebeck coefficient at σ_{\min} is mostly different from zero:

$$\alpha_i = \frac{1}{2}(\alpha_+ + \alpha_-) = (k/2e) \ln(N_+ e^{A_+} \mu_+ / N_- e^{A_-} \mu_-). \quad (10)$$

Jonker has shown¹⁰ that it is often useful to combine the expressions for α and σ into an equation

$$\alpha = \pm \frac{k}{2e} \left(\frac{E_g}{kT} + A_+ + A_- \right) \left[1 - \left(\frac{\sigma_{\min}}{\sigma} \right)^2 \right]^{1/2} - \frac{k}{e} \ln \left(\frac{\sigma}{\sigma_{\min}} \left\{ 1 \pm \left[1 - \left(\frac{\sigma_{\min}}{\sigma} \right)^2 \right]^{1/2} \right\} \right) + \alpha_i, \quad (11)$$

where “+” and “-” signs are valid for $\sigma_+ \geq \frac{1}{2} \sigma_{\min}$ and $\sigma_- \geq \frac{1}{2} \sigma_{\min}$, respectively. From this equation it follows that the shape and dimensions of an α vs $\ln(\sigma/\sigma_{\min})$ plot depend only on the parameter $\epsilon = E_g/kT + A_+ + A_-$. The term α_i causes a shift of

the symmetry axis of the curve with respect to the $\alpha = 0$ axis. Using such plots of α vs $\ln \sigma$ one is able to compare data obtained from different samples. The extrinsic conduction regions are easily recognized by straight lines in this curve. If the temperature coefficients of N and μ^{-1} are equal, as is approximately the case for band conduction, and if A is temperature-independent, one finds that the straight lines coincide for different temperatures.

III. EXPERIMENTAL METHOD

Electrical conductivity measurements and Seebeck coefficient measurements were performed on n -type as well as p -type single crystals of YIG. The crystals were grown from a PbO-PbF_2 flux. To obtain n -type or p -type behavior iron (Fe^{3+}) or yttrium (Y^{3+}) ions were replaced by small amounts of Si^{4+} , Zn^{2+} , or Ca^{2+} . The crystals further contain lead (Pb^{2+}) and possibly fluorine (F^-), which are incorporated from the flux. Table I gives the results of a chemical analysis of the single crystals used. Pb, Ca, and Zn were determined from atomic-absorption measurements; for Si and F a photometric analysis was used.¹⁴ The table also gives the total concentrations of foreign donors N_d and foreign acceptors N_a . It is seen that the crystals are strongly compensated. Apart from the above mentioned ions native donors are also present with concentrations of comparable magnitude [(0-0.03)/formula unit].¹⁵ The specific resistivity at 300 K is higher than $10^{10} \Omega \text{ cm}$ for samples 1 and 2, $\sim 10^4 \Omega \text{ cm}$ for sample 3, and 10^5 - $10^6 \Omega \text{ cm}$ for sample 4.

Samples with typical dimensions of $8 \times 5 \times 0.4 \text{ mm}^3$ were cut, polished, and subsequently cleaned in boiling HCl and trichlorethylene, after which Pt contacts of approximately $0.5 \mu\text{m}$ thickness were sputtered on the end faces. Earlier investigations with the four-point method have shown that such layers provide good Ohmic contacts suitable for high-temperature measurements.¹¹ In Fig. 1 a schematic drawing of the measuring cell is shown.

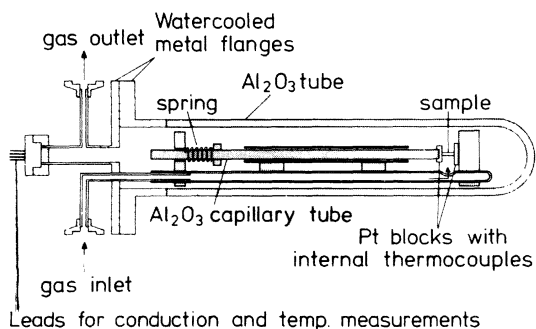


FIG. 1. Schematic drawing of the cell used for measurements of electrical conductivity and thermoelectric power.

The sample is placed between two spring-loaded Pt blocks inside a gas-tight alumina tube, which is again situated inside a SiC furnace. The Pt blocks are both connected to the outside of the cell via a Pt wire and via a Pt, Pt-10%-Rh thermocouple.

The Pt wires were used to carry the current for the dc conductivity measurements, while the thermocouples were used for both the measurement of the voltage drop across the sample and the temperature measurement at the end faces of the sample. During the experiments a constant gas flow was maintained through the measuring cell. Changes in the oxygen partial pressure were made by varying the composition of the O_2 - N_2 gas mixture. Zirconia oxygen gauges (Philips PW 9620) were used to determine continuously the oxygen partial pressure at the inlet and outlet of the measuring cell. The small internal gas volume of the cell enabled the oxygen pressure to be changed quickly, so that the response time of the conductivity could be measured. The use of these dynamic conductivity measurements for determining the oxygen diffusion rate will be described separately.¹²

The conductivity was determined from the voltage drop across the sample with constant current passing through it. Both polarities were always used. The current was kept low so that the voltage drop did not exceed 200 mV. The current-voltage relationship was found to be linear and no polarization effects were observed.

The Seebeck coefficient was obtained from the potential difference ΔV between the two Pt wires of the thermocouples attached to the Pt blocks at the end faces of the sample. The temperature difference over the sample was varied by changing the position of the measuring cell in the furnace. Because of deviations between the two thermocouples the measured temperature differences ΔT could be different from the actual one. The Seebeck coefficient was therefore obtained from the slope of the resulting linear dependence of ΔV on ΔT . The average temperature of the sample was kept constant within 1.5 K, while the variation in ΔT was about 15 K.

TABLE I. Concentrations of dopants and impurities in atoms/(formula unit).^a N_d and N_a are the sum of foreign donor and acceptor concentrations, respectively.

Sample	Pb	Ca	Zn	Si	F	N_d	N_a
1	0.020	0.017	...	0.021	...	0.021	0.037
2	0.008	0.001	0.012	0.001	...	0.001	0.020
3	0.037	0.003	...	0.081	0.001	0.082	0.040
4	0.022	0.001	...	0.027	0.008	0.035	0.023

^a 1 atom/(formula unit) = $4.22 \times 10^{21} \text{ cm}^{-3}$.

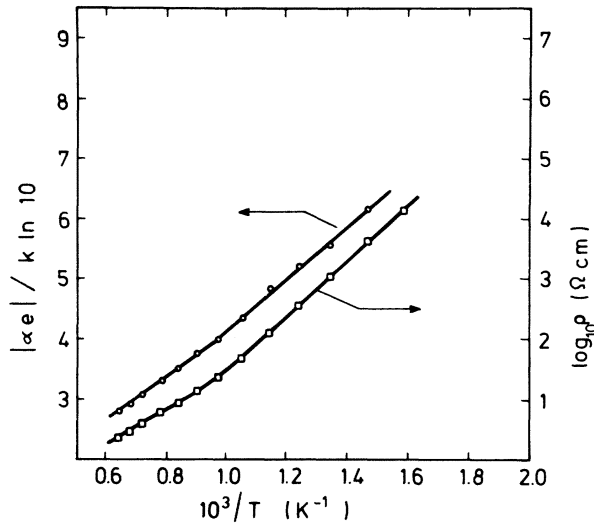


FIG. 2. Absolute value of the reduced Seebeck coefficient and the logarithm of the resistivity of *p*-type YIG (sample 1).

IV. EXPERIMENTAL RESULTS

A. Extrinsic conduction regions

In Figs. 2–5 the reduced Seebeck coefficients $\alpha' = |\alpha e|/k \ln 10$, and the logarithm of the specific resistance ρ are shown as a function of the reciprocal temperature. Figures 2 and 3 give the results for a Ca-doped crystal (sample 1, Table I) and for a Zn-doped crystal (sample 2, Table I). Both crystals show *p*-type behavior. In Figs. 4 and 5 the results are given for *n*-type Si-doped crystals (samples 3 and 4, Table I). The measurements were all performed at an oxygen partial pressure of 1 atm. In order to obtain reproducible results

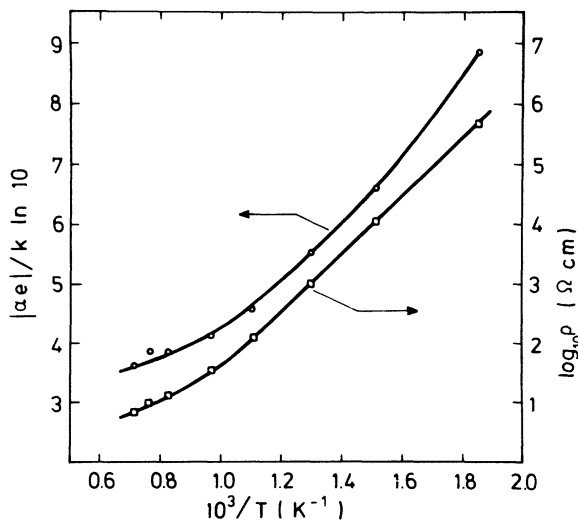


FIG. 3. Absolute value of the reduced Seebeck coefficient and the logarithm of the resistivity of *p*-type YIG (sample 2).

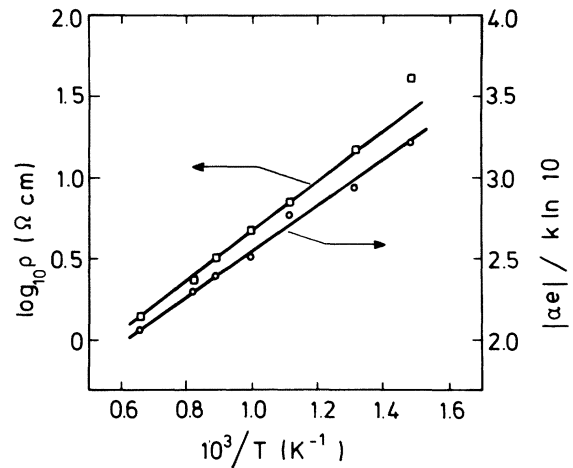


FIG. 4. Absolute value of the reduced Seebeck coefficient and the logarithm of the resistivity of *n*-type YIG (sample 3).

the samples were heated for at least 24 h at 1300–1400 °C before the measurements started. A considerable change in the resistivity was in some cases observed during this annealing treatment (at a fixed temperature and at an oxygen pressure of 1 atm). Similar irreversible changes were also found to occur during weight measurements with the aid of a thermobalance.¹⁶ Further investigations of the origin of these changes are in progress. Since these precautions were not taken for the measurements on sample 2 the resulting curves given in Fig. 3 for this crystal are less reliable.

The observation of approximately equal slopes in Figs. 2–5 for α' and $\log_{10}\rho$ for both *p*-type and *n*-type crystals shows that we have extrinsic conduction, and that the changes in α' and $\log_{10}\rho$ are mainly due to the temperature dependence of *p* (or *n*).

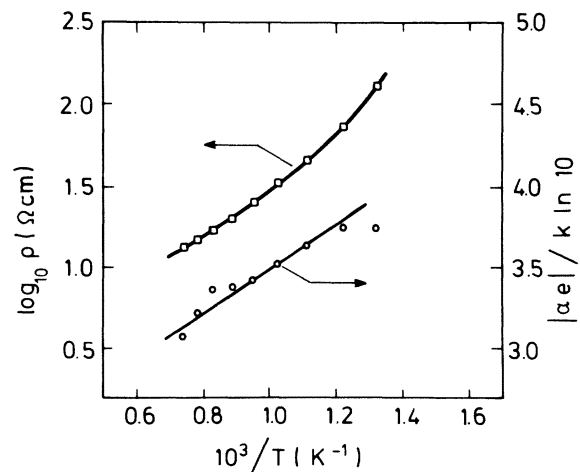


FIG. 5. Absolute value of the reduced Seebeck coefficient and the logarithm of the resistivity of *n*-type YIG (sample 4).

A further discussion of these results will be given in Sec. V and VI.

B. Intrinsic conduction region

Measurements in the intrinsic conduction region were performed on *p*-type samples, which were exposed to a gas mixture of varying oxygen partial pressures. The points along the lines a, b, c, and d in Fig. 6 show results at four different temperatures. The calculated curves (solid lines) shown in this figure will be discussed in Sec. V. The measurements represented by the curves a–d started with the sample in equilibrium at 1 atm of oxygen pressure. When the oxygen partial pressure is lowered the concentration of oxygen vacancies and hence the total donor concentration increases. This leads to a decrease in the number of holes. The arrow in Fig. 6 shows the direction in which α and σ change as a result of the lowering of the oxygen partial pressure. At low temperatures and $P_{O_2} = 1$ atm we find an extrinsic conduction, while at higher temperatures, especially at a low oxygen partial pressure, we are in the intrinsic region. The α , σ range that can be covered in this way, however, is rather restricted since measurements at pressures $P_{O_2} < 10^{-6}$ atm cause irreversible changes, that is to say even after a long time we do not get back the original α and σ values when P_{O_2} is reset at 1 atm (at a fixed temperature). The reason is probably the decomposition of the garnet into orthoferrite and magnetite. Measurements on a thermobalance indicate that such a decomposition starts at $P_{O_2} \approx 10^{-4}$ atm at 1240 °C.¹⁶

In an earlier publication¹¹ we presented similar graphs of α and σ . The measurements of the Seebeck coefficient were not made as described in Sec. III, but were based on a single temperature-dif-

ference measurement, leading to too high values of α , as given in Fig. 2 of Ref. 11. The present values of σ_{\min} , however, agree excellently with the earlier data. From a plot of $\ln \sigma_{\min}$ vs T^{-1} we obtain the relation

$$\sigma_{\min} = \sigma_0 e^{-E/kT}, \quad (12)$$

where $\sigma_0 = (6.0 \pm 0.13) \times 10^3 (\Omega \text{ cm})^{-1}$, and $E = \frac{1}{2} E_g = 1.43$ eV.

V. ANALYSIS

As discussed in Sec. II, a convenient compilation of our data can be given in an α - σ plot. In Fig. 6 the results are summarized in this so-called "Jonkers pear." The points with positive α values are by definition those of *p*-type samples, while negative Seebeck coefficients indicate *n*-type samples. The experimental points were obtained on the samples 1–4 (Table I). We have also included in this plot three points measured by Ksendzov *et al.*⁶ on silicon-doped YIG crystals. The points used in Figs. 2–5 are situated on the straight lines *CB* and *DB*, which represent extrinsic behavior. Furthermore the curves *CB* and *DB* fit to points obtained from a wide temperature interval, viz., 600–1500 K. This is important since the straight lines shift with temperature if the mobility is thermally activated. From the uncertainty in the position of these lines we estimate that the maximum value of a possible activation energy of the mobilities must be ≤ 0.1 eV. A similar conclusion can be obtained from Figs. 2–5. The differences in the slopes of the α' and $\log_{10} \rho$ curves are in all cases less than 0.08 eV.

From the position of the symmetry axis of Fig. 6 we find $\alpha_i = 75 \mu\text{V/K}$. Using Eq. (10) we then have

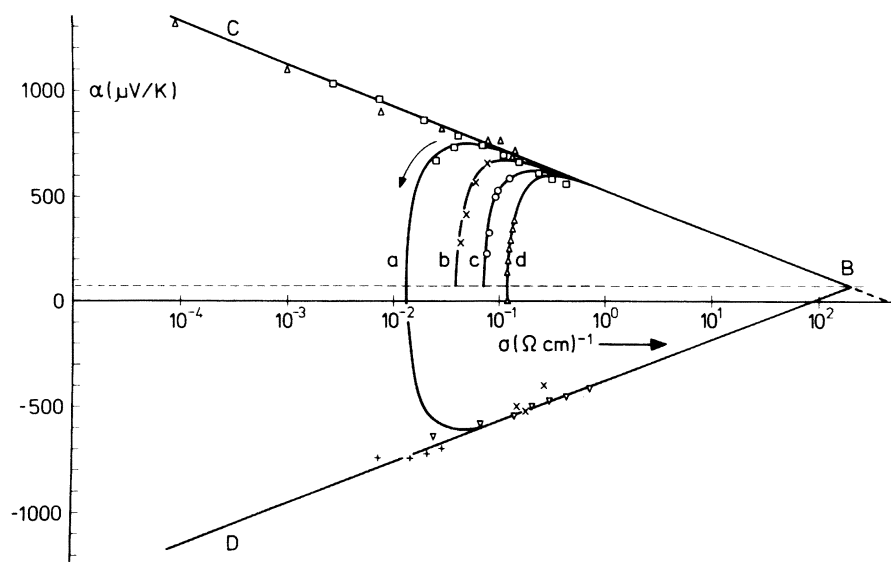


FIG. 6. Seebeck coefficient—conductivity plot for different YIG crystals. Positive α values represent *p*-type samples: \circ , \times , \square , sample 1; \triangle , sample 2. Line a, $T = 1265$ K; b, $T = 1378$ K; c, $T = 1451$ K; d, $T = 1514$ K. Along the lines a–d the temperature is kept constant and the oxygen partial pressure is reduced in the direction indicated by the arrow. For points along the lines *BC* and *BD* the oxygen partial pressure is kept constant at 1 atm. Negative α values represent *n*-type samples: ∇ , sample 3; $+$, sample 4; \times , literature data of Ref. 6.

$$N_+e^{A+\mu_+}/N_-e^{A-\mu_-} = 5.7. \quad (13)$$

As shown in Eq. (11) the shape and dimensions of the pear are fully determined by the parameter $\epsilon = E_g/kT + A_+ + A_-$. Using the relation

$$\epsilon = \ln(\sigma_B/\sigma_{\min})^2 + \ln 4, \quad (14)$$

where σ_B is the conductivity at the point *B*, we obtain from our data the value of ϵ as a function of temperature:

$$\epsilon = 3.31 \times 10^4/T - 5.42. \quad (15)$$

Here the coefficient to T^{-1} equals E_{g0}/k ($E_{g0} = 2.85$ eV),¹¹ while the constant term gives us a relation between the temperature coefficient of the band gap and the transport constants:

$$\beta/k + A_+ + A_- = -5.42. \quad (16)$$

We have used Eqs. (15) and (11) to calculate the α - σ curves at four different temperatures. These curves are shown by the solid lines a-d in Fig. 6. The agreement with the experimental data, which were obtained by varying the partial oxygen pressure, is seen to be quite good.

A relation between β , the densities of states, and the mobilities can be obtained from the value of the coefficient σ_0 in Eq. (12). Using Eq. (9) we get

$$\mu_+\mu_-N_+N_-e^{-\beta/k} = 3.52 \times 10^{44} \text{ (V sec cm)}^{-2}. \quad (17)$$

The equations (12), (16), and (17) allow a determination of the product μ_+Ne^A for holes and electrons separately. We find

$$\mu_+N_+e^{A+} = 3.0 \times 10^{21} \text{ (V sec cm)}^{-1}, \quad (18a)$$

$$\mu_-N_-e^{A-} = 5.2 \times 10^{20} \text{ (V sec cm)}^{-1}. \quad (18b)$$

We shall comment on these results in the concluding section.

More information can be obtained from the temperature dependence of the Seebeck coefficient. As discussed in Sec. II the product ge^A and the ionization energy E_a may be determined using Eq. (8). A quantitative analysis seems however not possible for our *p*-type samples. The slopes of the α' vs T^{-1} curves shown in Figs. 2 and 3 are not independent of the temperature, but increase with decreasing temperature. This indicates that E_F is not determined by Eq. (7). A comparison between the room-temperature resistivities of samples 1 and 2 ($\rho \approx 10^{10} \Omega \text{ cm}$) indicates that a considerable (but unknown) number of native donors are very probably present. The difference $N_a - N_d$ is then much reduced from the values determined by Table I and the relation $p \ll N_a - N_d$ may not be valid in the present temperature range. For the *n*-type samples the data for sample 3 only seem reliable

enough for a quantitative analysis of the temperature dependence. Referring to the discussion in Sec. VI, we assume that $n \ll N_d - N_a$ and that the counterpart of Eq. (8) for *n*-type samples is applicable. From the slope of the α' curve given in Fig. 3 we obtain $E_d = 0.28$ eV and from the intercept at $T^{-1} = 0$ (neglecting native donors) we find

$$A_- + \ln g_- = 2.7. \quad (19)$$

Here g_- is the degeneracy factor of the Si centers. It should be noted that the presence of native donors in a concentration of 0.02/(formula unit) only changes the right-hand side of Eq. (19) slightly (to 3.1). We have, however, no reason to assume that native donors of such a concentration are present in *n*-type YIG because σ_- depends very little on the oxygen partial pressure.

VI. DISCUSSION AND CONCLUSIONS

In this section we shall discuss our experimental results in terms of the localized hopping model mentioned in the Introduction, the small-polaron model, and the large-polaron model.

In the localized model for YIG the number of charge carriers is supposed to be independent of the temperature and equal to the number of Fe^{2+} or Fe^{4+} ions, while the thermally activated behavior of the conductivity is attributed to the drift mobility only. Our experimental results are, however, inconsistent with this model for both *n*- and *p*-type YIG. We found that plots of $\log_{10}\rho$ and α' vs T^{-1} show parallel lines or equivalently that the straight lines *CB* and *DB* in Jonker's pear are independent of temperature (and furthermore of sample). The temperature dependence of σ can therefore only be explained by a thermal generation of the (free) charge carriers. Because the activation energy of σ for Si-doped YIG at room temperature is approximately the same (~ 0.3 eV) as found for the present temperature range, it seems reasonable to suppose that this mechanism explains the temperature dependence of σ down to 300 K. A consequence of the lack of applicability of the localized hopping model seems to be that the concepts of Fe^{2+} or Fe^{4+} ions in YIG are not very meaningful.

However, our experimental results do not exclude the possibility of a small activation energy ($\leq kT$) of the mobility, and an estimate of the mobilities show that these (μ_+ and μ_-) are relatively small. We shall therefore discuss our results on the basis of the small-polaron model and the large-polaron model. The expressions given in Sec. II and used in Sec. V apply for both models¹⁷ and the numerical results presented in Eqs. (18a), (18b), and (19) form the basis for the discussion of these

models.

Most information has been obtained for n -type YIG, which we consider first. The effective density of states depends on the width ($2W$) of the lowest conduction band, supposedly derived from octahedral iron $t_{2g}(\text{Fe}^{2+})$ states.¹⁵ If the small-polaron model is applicable the width should be less than $\frac{1}{2}kT$ and allowing a factor of 2 for spin degeneracy the effective density of states $N_- = 2/(\text{formula unit})$, or $N_- = 8.4 \times 10^{21} \text{ cm}^{-3}$. For the small-polaron model the heat of transfer is negligibly small and setting $A_- = 0$ and using the value of N_- just given we find $\mu_- = 0.06 \text{ cm}^2/\text{V sec}$ and $g_- = 15$. These numbers do not support the small polaron model very much. An upper limit for μ is given by $\mu \ll 0.1 \text{ cm}^2/\text{V sec}$ and the found value of μ_- is therefore very large. The expected value of the spin-degeneracy factor for single ionizable donor impurities (like Si^{4+} impurities in YIG) is 2,¹³ and $g_- = 15$ seems rather high. The almost lack of temperature dependences for the product $\mu_- N_- e^{A_-}$ also does not support the small-polaron hopping model, but does not exclude it, because the temperature dependence of μ can be both positive and negative depending on the interaction of the polaron with the lattice.^{18,19} Finally optical measurements by Wemple *et al.* indicate that the bandwidth is much larger than kT .²⁰ From studies of the optical absorption and reflection and their derivatives in iron garnets, the lowest charge transition was found at the energy 2.88 eV, in good agreement with the band-gap energy (2.85 eV). This transition has a width at half-maximum of 0.3 eV.

Let us next consider the large-polaron model, again for n -type YIG. The temperature independence of $\mu_- N_- e^{A_-}$ is in agreement with this model. The transport constant A_- can be supposed to be equal to 2 and using Eq. (19) we find $g_- = 2$, which is the expected value for g . In order to determine the mobility and see if this value is consistent with the large-polaron model we have to estimate N_- . If we assume a parabolic band and a bandwidth of $2W$ ($\gg kT$) the effective density of states is reduced with approximately a factor of $(kT/2W)^{3/2}$ from that for the small-polaron model. Because photoemission measurements⁹ and optical-absorption measurements¹⁵ have shown that we have broad bands as the highest valence bands, we tentatively set W to the value quoted above, i.e., $W = 0.3 \text{ eV}$. At $T = 1000 \text{ K}$ we then get $N_- = 4.6 \times 10^{20}$

cm^{-3} and $\mu_- \approx 0.15 \text{ cm}^2/\text{V sec}$. This value for μ_- is rather low for the large-polaron model predicting $\mu \approx 0.7 \text{ cm}^2/\text{V sec}$ for a total bandwidth of 0.6 eV.¹⁷ We have used the given values of N_- and μ_- to compare n with the donor and acceptor concentrations and find $n \ll N_d - N_a$ as required for the use of Eq. (8) in our data analysis.

For p -type YIG there is, as mentioned above, strong evidence for a broad band as the highest valence band. If we compare Eqs. (18a) and (18b) we find even less support for the applicability for the small polaron model for p -type than for n -type YIG, in agreement with the absence of a localized valence band as the highest band. For a parabolic band with effective mass m^* we have at $T = 1000 \text{ K}$ $N_+ \approx 1.5 \times 10^{20} (m^*/m_0)^{3/2} \text{ cm}^{-3}$. Setting $A_+ = 2$ we then get $\mu_+ = 0.5 (m/m^*)^{3/2} \text{ cm}^2/\text{V sec}$, which seems a low value for broadband conduction ($\mu \geq 2.5 (m/m^*)^{1/2} \text{ cm}^2/\text{V sec}$).¹⁷ The temperature independence of $\mu_+ N_+ e^{A_+}$ supports the band model, however.

We have so far not discussed Eq. (16) relating the temperature coefficient of the band gap and the transport constants. Assuming both A_+ and A_- have the value 2 we get $\beta = -8.1 \times 10^{-4} \text{ eV/K}$, while $A_+ = A_- = 0$ would give us $\beta = -4.7 \times 10^{-4} \text{ eV/K}$. An optical investigation of the temperature dependence of the lowest-charge-transfer transition determining β would be very useful determining the sum $A_- + A_+$ independently.

On the basis of the discussion given above we have the following conclusions: (a) The localized hopping model is not applicable for YIG at $600 \text{ K} < T < 1500 \text{ K}$ (and probably down to 300 K), because the thermal generation of charge carriers gives the main contribution to the temperature dependence of σ for both n - and p -type YIG. The concepts of Fe^{2+} and Fe^{4+} ions in YIG should therefore be avoided. (b) The small-polaron model does not give a reasonable explanation of the experimental data. (c) The large-polaron model describes the data reasonably well, but the estimated mobilities are rather low for this model. (d) An unambiguous determination of the parameters μ , N , A , β , and g from the four relations [Eqs. (16), (18a), (18b) and (19)] has not been possible and awaits further experimental evidence.

ACKNOWLEDGMENT

The authors wish to thank P. G. T. Boonen for his technical assistance.

¹J. Verweel and B. J. M. Roovers, *Solid State Phys. Electron. Telecommun.* **3**, 475 (1960).

²D. L. Wood and J. P. Remeika, *J. Appl. Phys.* **37**, 1232 (1966).

³U. Enz, R. Metselaar, and P. J. Rijnierse, *J. Phys.* **32**, C1-703 (1971).

⁴J. F. Dillon, Jr., E. M. Gyorgy, and J. P. Remeika, *J. Appl. Phys.* **41**, 1211 (1970).

- ⁵D. Elwell and A. Dixon, *Solid State Commun.* 6, 585 (1968).
- ⁶Ya M. Ksendzov, A. M. Kotel'nikova, and V. V. Makarov, *Fiz. Tverd. Tela* 15, 2343 (1973) [*Sov. Phys.-Solid State* 15, 1563 (1974)].
- ⁷R. E. Fontana and D. J. Epstein, *Mater. Res. Bull.* 6, 959 (1971).
- ⁸P. K. Larsen and R. Metselaar, *Phys. Rev. B* 8, 2016 (1973).
- ⁹P. K. Larsen, R. Metselaar, and B. Feuerbacher, *AIP Conf. Proc.* 29, 668 (1976).
- ¹⁰G. H. Jonker, *Philips Res. Rep.* 23, 131 (1968).
- ¹¹R. Metselaar and P. K. Larsen, *Solid State Commun.* 15, 291 (1974).
- ¹²R. Metselaar and P. K. Larsen, *J. Phys. Chem. Solids* 37, 599 (1976).
- ¹³J. S. Blakemore, *Semiconductor Statistics* (Pergamon, Oxford, 1962).
- ¹⁴These single crystals and the analysis results were placed at our disposal by W. Tolksdorf.
- ¹⁵P. K. Larsen and R. Metselaar, *J. Solid State Chem.* 12, 253 (1975).
- ¹⁶R. Metselaar and M. A. H. Huyberts (unpublished).
- ¹⁷A. J. Bosman and H. J. Van Daal, *Adv. Phys.* 19, 1 (1970).
- ¹⁸T. Holstein, *Ann. Phys.* 8, 325 (1959); 8, 343 (1959).
- ¹⁹D. Emin, *Phys. Rev. B* 4, 1321 (1971); 4, 3639 (1971).
- ²⁰G. H. Wemple, S. L. Blank, J. A. Seman, and W. A. Biolsi, *Phys. Rev. B* 9, 2134 (1974).

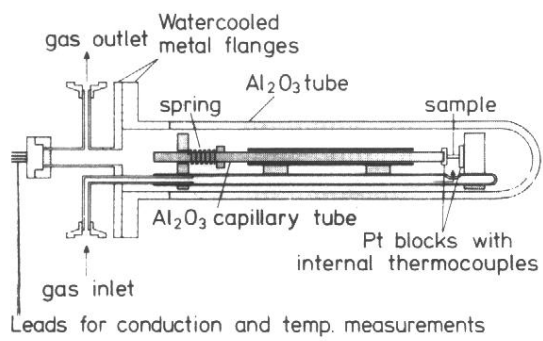


FIG. 1. Schematic drawing of the cell used for measurements of electrical conductivity and thermoelectric power.